In Situ MONITORING AND UNIVERSAL MODELLING OF SACRIFICIAL PSG ETCHING USING HYDROFLUORIC ACID

Jianqiang Liu & Yu-Chong Tai
Electrical Engineering, 116-81, Caltech, Pasadena, CA 91125

Jiajing Lee , Kim-Cheok Pong, Yitshak Zohar & Chih-Ming Ho
MANE, UCLA, Los Angeles, CA 90024

Abstract

A video system is designed to monitor the etching of sacrificial phosphosilicate-glass (PSG) microchannels in-situ accurately using hydrofluoric acid (HF). An universal model, which predicts accurately the etching length vs. time over a wide range of HF concentration (3-49 wt%), is identified. In addition to diffusion, this model is based on a first-and-second order chemical reaction mechanism. It is found that the PSG microchannel etching rate in HF is sensitive to channel thickness but not width. Finally, bubble formation and movement inside the etched microchannels are observed. Most of the generated bubbles are mobile and can enhance the etching rate.

1. Introduction

Chemical etching of sacrificial layers is a widely used technique in surface micromachining[4]. For example, silicon dioxide or PSG can be easily etched in HF-based solutions with very high selectivity over silicon and silicon nitride. In fact, etching of silicon dioxide in HF was studied as early as 1913[5]. Readily, many chemical models as well as calibrated etching rates of differently doped oxides in HF are available[1, 7, 9, 10]. However, these works were derived from etching experiments intentionally designed to be in reaction-limited regimes. They are useful when the etching length of the sacrificial layer is short (< 100 μm), thus reactive chemicals can always be sufficiently supplied at the etching front. Therefore, the etching time can be calculated just using the reaction-limited etching rate. However, if the etching length is long such as in channel etching, reactive chemicals at the etching front may be depleted. The etching rate then is dominated by diffusion mechanism. As a result, a good model has to include both chemical reaction and diffusion. In addition, such a model should also be applicable to a wide range of concentrations. A model which satisfies all these criteria will thereafter be called an universal model.

Recently, Monk et. el.[11, 12] reported the first study of PSG etching in microchannels using HF-based solutions. Both Deal-Grove and non-first-order models have been examined. It was shown that under specific concentrations both models can fit etching data well. However, no information on the applicability of the models over a wide range of HF concentration was provided. In fact, from our data, we have found that neither model is universal. Here, we present our work to find a universal model which includes a first-and-second order chemical-reaction mechanism.

2. Microchannel Fabrication and Experimental Setup

Straight one-dimensional PSG microchannels of different dimensions are fabricated. Fig. 1a shows the cross-section of a channel. One end of each channel is completely sealed, while the other end is an etching window. The typical length of the channels is 3000 μm. The widths of these channels range from 2 μm to 200 μm. The height of the channels, which is also the PSG thickness, is 1 μm if not specifically mentioned in this paper. To facilitate the measurement of the etching lengths under a microscope, scales with 10 μm per division were integrated on the chip. Fig. 1b is a photograph of three channels which have been etched partially in HF solution.

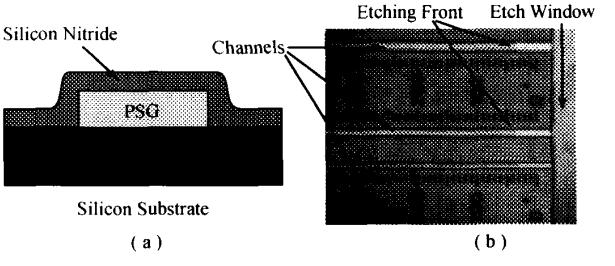

Figure 1: (a) Cross-section schematic of a microchannel. (b) Photograph of three microchannels topview. Each division of the ruler is 10μm.

The fabrication of the microchannels starts with 4-inch silicon wafers. First, a 1-μm-thick LPCVD PSG layer is deposited at 450°C. A thermal annealing step at 1000°C for one hour is to densify the PSG. The PSG layer then is patterned, and an 1.2-μm-thick LPCVD low-stress silicon nitride is deposited at 820°C. Finally, etching windows are opened using SF_6 plasma. The sacrificial PSG layer has a phosphorus concentration of 6%. The uniformity of the PSG across the wafer is about $\pm 5\%$.

Etching experiments are carried out under an *in situ* monitoring system which is schematically shown in Fig. 2. This monitoring system consists of a microscope, a video camera,

0-7803-0957-2/93 $3.00 © 1993 IEEE

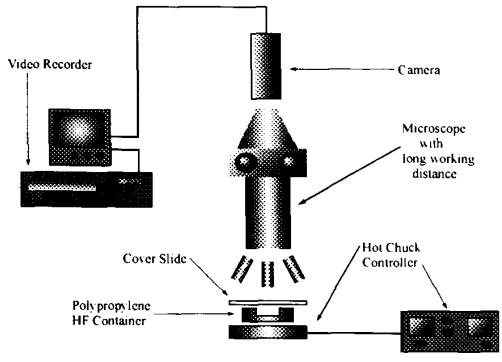

Figure 2: Schematic of experimental setup. Vapor condensation on the lens is avoided by using a plastic cover on the HF container.

a tape recorder, and a temperature-controlled hot chuck. Etching of the chip is performed in a specially designed polypropylene container with a transparent plastic cover slide. A chip is fixed inside the container and HF solution is injected into the container to start the PSG etching. The whole process is video-recorded. Later on, data of channel etching length vs. time are read from tape. The hot chuck is used only for study of temperature effects.

3. Etching Models

To model the etching, we make the following assumptions: the channel etching is one-dimensional; the diffusion coefficient is a constant; all the liquid has a constant density; the heat generation at the etching front is negligible; the reaction products has no chemical effects on the reaction-chemical distribution. We also assume that the overall chemical reaction is

$$6HF + SiO_2 \rightleftharpoons H_2SiF_6 + 2H_2O \ . \tag{1}$$

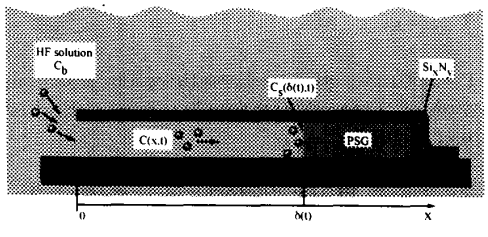

Figure 3: Conventions used in our model formulation.

Using the coordinates defined in Fig. 3, the continuity equation for reaction chemical concentration is,

$$\frac{\partial C}{\partial t} + u\frac{\partial C}{\partial x} = D\frac{\partial^2 C}{\partial x^2} \ . \tag{2}$$

where u is the flow velocity, $C(x,t)$ is the concentration of the reaction chemical and D is the diffusion constant. The diffusive flux, J_d, is then given by Fick's first law,

$$J_d = -D\frac{\partial C}{\partial x} \ . \tag{3}$$

We wish to determine the relative magnitude of the convection and diffusion term in Eq. (2). According to Eq. (1), there is a volume change of the liquid at the etching front that for the etching of every mole of SiO_2, there is a generation of 2 moles of H_2O. The molecular weight, [MW], of SiO_2 and H_2O is 60 and 18 g/mole, respectively. Their corresponding densities, ρ, are 2.1 and 1 g/cm^3. Thus, for every mole of SiO_2 etched, the solid volume decreases by 28.6 cm^3, but the liquid volume increases by 36 cm^3. The net volume change then is an increase of 7.4 cm^3/mole ($\sim$ 26%). The velocity of the etching front is found experimentally to be 20 μm/min for PSG in 49% HF. Thus, the back-flow velocity, u, caused by volume increase is about 6 μm/min. With a $D \sim 3 \times 10^{-5}$ cm/sec[15], the order-of-magnitude estimate of the ratio between the convective and diffusion terms is,

$$u\frac{\partial C}{\partial x} \Big/ D\frac{\partial^2 C}{\partial x^2} \approx \frac{u\delta(t)}{D} \sim 3 \times 10^{-5}\frac{\delta(t)}{\mu m} \ .$$

It can be concluded that for $\delta(t)$ up to several thousand microns, the convection term in the continuity equation is negligible. This, however, may not be true if forced-convection sources, such as bubble formation, exist.

Neglecting the convective term, the governing equation now becomes,

$$\frac{\partial C}{\partial t} - D\frac{\partial^2 C}{\partial x^2} = 0 \ . \tag{4}$$

The boundary conditions are,

$$\begin{aligned} C(0,t) &= C_b \ , \\ C(\delta(t),t) &= C_s \ , \end{aligned} \qquad \text{for} \quad t > 0 \ , \tag{4.a}$$

where C_b is the bulk HF concentration, and C_s is the etching front concentration. To solve Eq. (4, 4.a), we need a third boundary condition which can be derived as follows. In a stoichiometric reaction, one has

$$J_{[SiO_2]} = \frac{1}{6}J_{[HF]} \ , \tag{4.b}$$

and the etching rate is proportional to the SiO_2 flux at the front,

$$\frac{d\delta}{dt} = J_{[SiO_2]}\frac{[MW]_{[SiO_2]}}{\rho_{[SiO_2]}} \ . \tag{4.c}$$

From Eq. (3, 4.b, and 4.c), the third boundary condition is,

$$\frac{d\delta}{dt} = -\frac{D_{[HF]}}{6}\frac{[MW]_{[SiO_2]}}{\rho_{[SiO_2]}}\frac{\partial C}{\partial x}\bigg|_{x=\delta(t)} \ , \tag{4.d}$$

where $D_{[HF]}$ is the diffusion constant of the HF molecule in the etching solution. Eqs. (4, 4.a, and 4.d) form the basis for the following models.

3.1 Diffusion Model

If the chemical reaction rate is very high, the etching speed of the microchannels is limited by diffusion. In this case, concentration of reactant chemicals at the etching front would be very low. In the extreme, $C_s = 0$. Eq. (4) with boundary conditions (4.a & d) then represent a standard one phase Stefan problem[3]. The solutions are,

$$C(x,t) = C_b - \frac{6\rho_{[SiO_2]}}{[MW]_{[SiO_2]}} A e^{A^2/4} \int_0^{\frac{x}{2\sqrt{Dt}}} e^{-\xi^2} d\xi \ , \quad (5)$$

$$\delta(t) = A\sqrt{Dt} \ , \quad (6)$$

where the constant A can be solved by,

$$A e^{A^2/4} \int_0^{\frac{A}{2}} e^{-\xi^2} d\xi - \frac{[MW]_{[SiO_2]}}{6\rho_{[SiO_2]}} C_b = 0 \ . \quad (7)$$

There are two good reasons to study the diffusion model. First, the diffusion model helps to justify a very important simplification that the HF concentration distribution inside the etched channel is linear as shown in Fig. 4a. Secondly, because $C_s = 0$ is assumed, Eq. (6) predicts the maximum etching length as a function of t. Alternatively, the best fit of the data to Eq. (6) gives the lower limit of diffusion coefficient, D_{min}. As shown in Fig. 4b, a lower limit of D of 1.2×10^{-5} cm^2/sec is found from our data. However, Fig. 4b also shows that the diffusion model is not an universal model. This is because in reality $C_s \neq 0$.

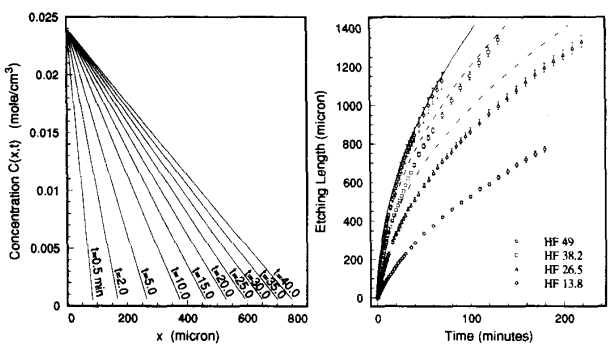

Figure 4: (a) Calculated concentration distribution along microchannels assuming $C_s = 0$. (b) Fitting of the diffusion model to experimental data with $D = 1.2 \times 10^{-5}$ cm^2/sec. Clearly, the diffusion model can not fit a wide range of HF concentration, hence is not universal.

3.2 Deal-Grove (D-G) Model

In the D-G model, the concentration in the channel is assumed to be linear as justified by diffusion model, so

$$J_d = -D\frac{\partial C}{\partial x} = D\frac{(C_b - C_s)}{\delta} \ . \quad (8)$$

Furthermore, the rate of chemical reaction is assumed to be linearly proportional to the etching front concentration,

$$J_{[HF]} = kC_s \ , \quad (9)$$

where k is the first-order reaction rate coefficient. $J_{[HF]}$ is the reaction flux of HF. In steady state, $J_d = J_{[HF]}$, the solution of the D-G model is[11],

$$\delta = -\frac{D}{k} + \sqrt{\left(\frac{D}{k}\right)^2 + \frac{DC_b[MW]_{[SiO_2]}}{3\rho_{[SiO_2]}} t} \ . \quad (10)$$

D-G model is a first-order chemical reaction model. This model fails to fit our etching experimental data as shown in Fig. 5.

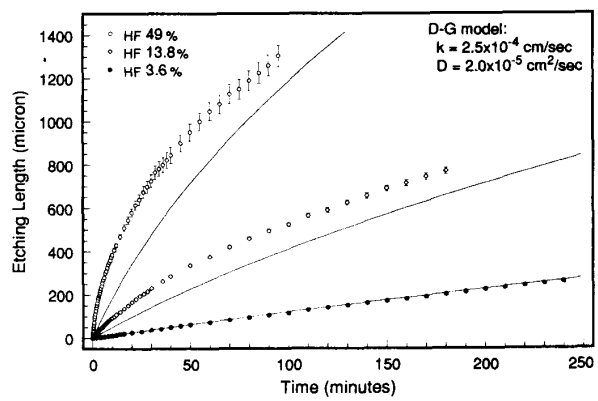

Figure 5: Fitting of D-G model to experimental data. Obveriously, D-G model is not universal.

3.3 Combined First-and-Second Order Model

In this model, the concentration distribution is also linear such that, in steady state,

$$J_{[HF]} = D\frac{(C_b - C_s)}{\delta} \ . \quad (11)$$

However, the reaction rate equation includes both a linear and a quadratic term,

$$J_{[HF]} = k_1 C_s + k_2 {C_s}^2 \ . \quad (12)$$

Solving Eq. (11) and (12), one has,

$$J_{[HF]} = \frac{1}{2k_2}\left(\frac{D}{\delta}\right)^2 \left(1 + b\left(\frac{\delta}{D}\right) - \varphi\right) \ . \quad (13)$$

where

$$b = k_1 + 2C_b k_2 \ , \quad (13.a)$$

$$\varphi = \sqrt{1 + 2b\left(\frac{\delta}{D}\right) + k_1^2\left(\frac{\delta}{D}\right)^2} \ . \quad (13.b)$$

Substitute Eq. (13) into Eqs. 4b and 4c, a first order differential equation can be derived as

$$\frac{d\delta}{dt} = a\left(\frac{D}{\delta}\right)^2 \left[1 + b\left(\frac{\delta}{D}\right) - \varphi\right] \ . \quad (14)$$

where $a = [MW]_{[HF]}/4\rho_{[SiO_2]}k_2$. This equation can be solved numerically. However, instead of searching for solutions of the form $\delta = f(t)$, one can integrate this equation from $\delta = 0$ at $t = 0$ to δ at time t to find:

$$t = \frac{D\left\{\varphi\phi + 2k_1^2\left(\frac{\delta}{D}\right) + b\left(k_1^2\left(\frac{\delta}{D}\right)^2 - 1\right)\right\}}{8aC_bk_1^2k_2(k_1 + C_bk_2)} - \frac{D}{2ak_1^3}\log\frac{\phi + k_1\varphi}{2(k_1 + C_bk_2)}, \quad (15)$$

where

$$\phi = k_1 + 2C_bk_2 + k_1^2\left(\frac{\delta}{D}\right). \quad (15.a)$$

Coefficients of k_1, k_2, and D can be determined experimentally. A non-linear least-square-fit method (*Levenberg-Marquardt method*[13]) is used to fit Eq. (15) to experimental data, and results are shown in Fig. 6.

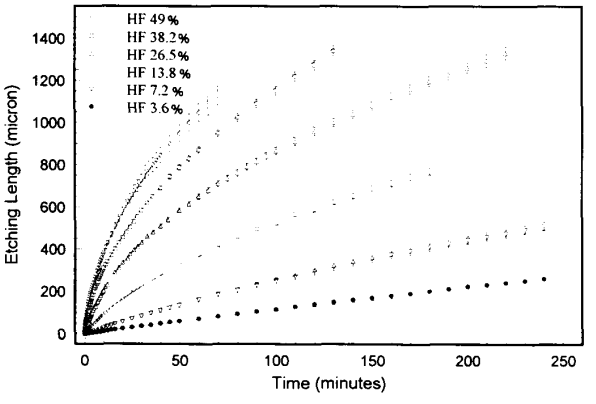

Figure 6: PSG channels etching with different HF concentration. Vertical bars show the scatter of different channel etching data. Solid lines are our model with parameter $k_1 = 1.2 \times 10^{-4}$ cm/sec, $k_2 = 6.5 \times 10^{-2}$ cm^4/mole·sec, and $D = 1.6 \times 10^{-5}$ cm^2/sec. A wide range of good fit is obtained.

In Fig. 6, bulk concentration, C_b, varies from 3.6 to 49 wt.%. The data are collected from many etching experiments with data scattering represented by the error bars. Clearly, this model fits all the data well using $k_1 = 1.2\times10^{-4}$ cm/sec, $k_2 = 6.5 \times 10^{-2}$ cm^4/mole·sec, and $D = 1.6 \times 10^{-5}$ cm^2/sec. Note that the diffusion constant, D, is indeed larger than D_{min} (1.2×10^{-5} cm^2/sec) predicted from the diffusion model.

Another useful equation relating C_s with δ can be derived from Eq. (12) and (13) which is,

$$C_s = \frac{-D - k_1\delta + D\varphi}{2k_2\delta}. \quad (16)$$

With Eq. (16), we can plot a etching rate vs. HF concentration curve at the etch front for each set of experimental data by taking time derivatives of the data shown in Fig. 6. Results are presented in Fig. 7. Since etching rate depends only upon concentration, all the data point should fall into a single smooth curve according to the formula expressed parametrically by Eq. (14) and (16). Again, the results in Fig. 7 confirms our model in predicting correct etching for all concentrations.

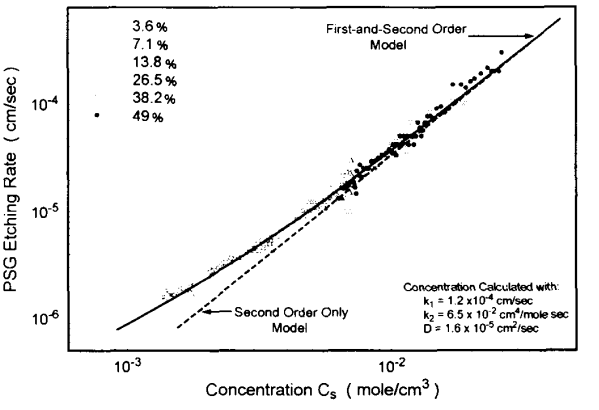

Figure 7: PSG etching rate dependence on concentration, C_s. Solid line represent the first and second order model with parameters shown in the graph.

Fig. 8 further shows concentration variation at the etching front. Initially, HF concentration drops very fast for high concentrated HF. After several hundreds microns, the concentration varies slowly as in low HF concentration.

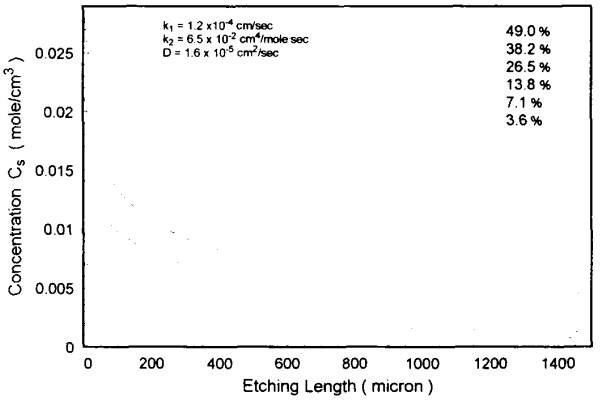

Figure 8: Concentration at the etching front.

Finally, Langmuir-Hinshelwood (L-H) chemical kinetic model ($r = -k_1[HF]/(1 + k_2[HF])$)[9] has also been proposed to predict etching process. We solved L-H and diffusion coupled model numerically. we have found that even with three fitting parameters, the L-H model fails to fit the data universally.

4. Discussion

4.1 Chemical Foundation for the Universal Model

As shown, among all the models, the combined first-and-second model is the only one which can fit universally. It clearly means, at low concentrations, the etching is dominated by a first order chemical reaction, and at high concentrations by a second order chemical reaction. In fact, Eq. (12) is reasonable from other chemistry studies which are summarized in the following.

It is known that aqueous HF solutions are characterized by the following equilibria[9],

$$HF \rightleftharpoons H^+ + F^- \ , \qquad (17.a)$$

$$2HF \rightleftharpoons H^+ + HF_2^- \ , \qquad (17.b)$$

$$\cdots \qquad \cdots$$

$$iHF \rightleftharpoons H^+ + H_{i-1}F_i^- \ . \qquad (17.c)$$

In equilibrium, many species such as, H^+, F^-, HF, HF_2, etc. can exist simultaneously. It has been shown that free fluoride can be excluded from one of the species responsible for the silicon dioxide etching[7, 9]. A rate equation of the form,

$$-r = A[HF] + B[HF_2^-] + C \ . \qquad (18)$$

was therefore proposed by Judge[7]. He concludes that the reaction with HF_2^- is about four to five times as fast as the reaction with HF. On the contrary, however, Kline[9] claims that rapid dissolution of silicates by hydrofluoric acid can be completely attributed to HF molecules. Nevertheless, neither can explain concentrated HF etching data. This problem may be solved using Eq. (17b) from which one can write

$$-r = C_1[H^+][HF_2^-] = C_1C_2[HF]^2 \ . \qquad (19)$$

This rate law was reported by Born[2] in 1979, and was added to Eq. (18) by Helms in 1991 in order to fit data collected using concentrated hydrofluoric acid[6]. Recently, Monk[12] used a non-first order rate law in his study of PSG etching by high concentrated HF and fit his data successfully. But it was not pointed out of what order the model was. In our work, it is found that the second order term is dominant at high HF concentration.

Finally, the etching rate of PSG (phosphosilicate glass) is different from that of SiO_2. The rates for variously doped SiO_2 in buffered HF solution have been reported by Kikuyama[8]. However, the mechanism that phosphorus doping changes the etching rate of silicon dioxide is still unclear. Kikuyama's study with doped oxide suggest that the etching difference between doped and undoped SiO_2 is caused by valence differences between silicon and the dopant elements. According to him, the role of phosphorus is to weaken silicon-oxygen bonds in the doped film thus facilitate the etching process. This agrees with the etching mechanism described by Prigogine[14]. A cautious conclusion, however, is that the basic chemistry is unaffected by the presence of phosphors. Therefore the rate law for SiO_2 etching should be applicable to PSG etching. This agrees with our modelling results where same chemical reaction mechanisms have been used for both SiO_2 and PSG.

4.2 Temperature Effect

During the course of data collection, we have found many factors which potentially can affect the reliability of our data. Temperature is one of these factors. Fig. 9a shows our preliminary experimental results of the etching length vs. time under different temperatures. It is interesting to see that higher temperature increases the etching speed at least at the beginning of the etching, which shows that the reaction constants are sensitive to temperature[7]. It is also interesting to see that after 300 μm channel etching, bubbles start to form and the etching lengths, after 100 minutes, are almost the same even at different temperatures. We believe that bubble-enhanced convection is the reason to explain this phenomenon.

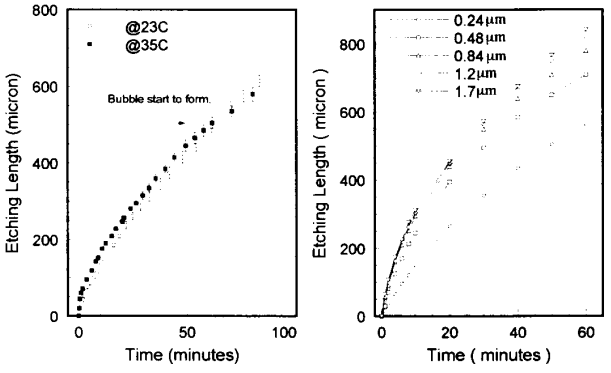

Figure 9: (a) PSG channels etching at different temperatures. (b) Five PSG channels of different thickness etching in 26.5 wt.% HF solution.

4.3 Size Effects

From our experiments, it is first observed that the width of microchannels does not affect etching speed for channels widths ranging from 4 μm to 200 μm as long as channel thickness is the same. On the other hand, thickness is found to have significant effects on the etching speed as shown in Fig. 9b. Samples with heights from 0.24 μm to 1.7 μm are etched in 26.5 wt% HF solution. Results show that thinner PSG channels are etched much slower than the thicker ones.

There are two possible reasons for the height dependence of etching rate; One is surface interaction between solid and liquid which may either increase or reduce etching rate. The other is that flow is involved in the etching. In this case, we would expect that the etching rate will increase with the channel height since the channels with larger cross-section tend to allow stronger fluid motion.

4.4 Bubble Generation

From *in-situ* monitoring channel etching, we have observed bubble forming and moving inside the channels. In KOH etching silicon, bubble formation has been reported[16].

Since the chemical reaction between SiO_2 and hydrofluoric acid does not generate gas product, it is not expected to see the bubbles. In fact, we have found no other reports on bubble formation in HF etching.

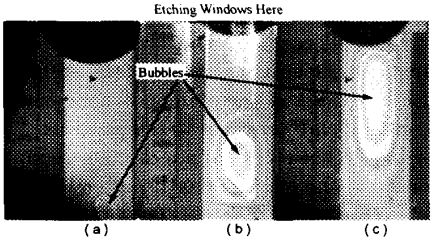

Figure 10: Bubble formation and its sequential movement. (a) A bubble forms near the etching front. (b) The bubble moves toward the etching window. (c) The bubble reaches the etching window. Note that the bubble grows in size during its movement.

From our experiments, it is found that bubbles always form certain time after etching begins. Once bubble formation is initialized, it will not stop by itself. In most of the cases, the bubbles grow in size inside the channel and move out of the channel repeatedly. Fig. 10 shows such a process of bubble forming. Effects of the bubbles on channel etching depend upon the size of the channels. Since bubbles are always in motion(they move out from the etching channel and, at the same time, expand in volume), microconvection can be induced if channels size are large, otherwise liquid is pushed out for a while in small channels. Thus there is a width threshold of about 10 μm. Above this, etching rate may speed up. Below this threshold, etching rate slows down.

Finally, we find that bubble formation is very sensitive to temperature. The generation rate and moving speed after bubble formation decrease with temperature. The lag time for bubble formation, however, increases with temperature decrease.

5. Conclusion

Four models are carefully examined here. Only the first and second order combined model fits universally with our experimental data with concentration range from 3.6 to 49 wt%. Results are summarized in Tab. 1. This universal model can be applied to silicon dioxide, doped or undoped, etching in HF solution.

Table 1. Summary of Models Comparison

Model	Model Parameters	Reaction Rate Law	Fitting Results
Diffusion Model (sec. 3.1)	D : diffusion Constant D_{min}=1.2 cm^2/sec	Chemical reaction proceeds in infinite speed. C_s=0	Not adequate
Deal-Grove Model (sec. 3.2)	D:diffusion constant. k: first-order reaction rate.	$J = kC_s$ Linear C(x,t)	Not adequate
Combined First and Second Order Model (sec. 3.3)	k_1 = 1.2x10^{-4}cm/s, k_2 = 6.5x10^{-2} D= 1.6x10^{-5}cm^2/s	$J= k_1C_s+k_2C_s^2$ Linear C(x,t)	Fit universally
Langmuir-Hinshelwood Model (sec. 3.3)	k_1, k_2, D	$J = k_1C_s/(1+ k_2C_s)$ Linear C(x,t)	Not adequate

Acknowledgement

This work is supported by AFSOR. We specially thank Mr. Amish Desai for his help in collecting etching data and Trevor Roper for help in fabrication.

References

[1] Avrom A. Blumberg, *J. Phys. Chem.*, vol. **63**, pp. 1129-1132,1959.

[2] H. Born, M. Prigogine, *J. Chim. Phys.*, 1979, Vol. **79**, pp. 540.

[3] John R. Cannon, *The One-Dimensional Heat Equation.* Addison-Wesley publishing company, 1984, Ch.17, pp. 281.

[4] L.S. Fan, Y.C. Tai, and R.S. Muller, *IEEE Trans. on Electron Devices*, 1988, Vol. **ED-35**, No. 6, pp. 724-730.

[5] A.Gautier & P. Clausmann, *Compt. rend.*, 1913, Vol. **157**, pp. 176.

[6] C. R. Helms, and B. E. Deal, *J. Vac. Sci. Technol. A*, 1992, Vol. **10**(4), pp. 806-811.

[7] John S. Judge, *Journal of The Electrochemical Society*; Solid State Science, November 1971, pp. 1772-1775.

[8] H. Kikuyama, M. Waki, I. Kawanabe and M. Miyashita, T. Yabune, and N. Miki, *J. Electrochem. Soc.*, 1992, Vol **139**(8), pp. 2239 -2243.

[9] William E. Kline & H. Scott Fogier, *Ind. Eng. Chem. Fundam*, 1981, **20**, pp. 155-161.

[10] T.A. Lober & R.T. Howe, in IEEE *Solid-State Sensors and Actuators Workshop*(IEEE, Hilton Head Island, SC,1988), pp. 59-62.

[11] David J. Monk et. al. *International Conference on Solid-State Sensors and Actuators: Transducers' 91* (IEEE, San Francisco, CA, 1991), pp. 647-650.

[12] David J. Monk et. al. *IEEE Solid-State Sensor and Actuator Workshop*(Hilton Head Island, South Carolina), 1992, pp. 46-49.

[13] William H. Press, Brian P. Fiannery, Saul A. Teukoisky & William T. Vetterling,*Numerical Recipes, The Art of Scientific Computing*[FORTRAN Version], pp. 550.

[14] M. Prigogine, and J. J. Fripiat, *J. Chem. Phys.*, 1979, Vol. **76**, pp. 26.

[15] Reid, et. al.,"The Preperties of Gases and Liquids."

[16] Osamu Tabata, Keiichi Shimaoka & Susumu Sugiyama, 1991 IEEE.